Neuroimaging of Phakomatoses

Doris D.M. Lin, MD, PhD,* and Peter B. Barker, DPhil*,†

The phakomatoses are congenital disorders manifesting with central nervous system and cutaneous abnormalities. The structures predominantly affected are those of ectodermal origin, including the skin, nervous system, and eyes. The 4 most common phakomatoses are neurofibromatosis (types 1 and 2), tuberous sclerosis, Sturge-Weber disease, and von Hippel-Lindau disease. Imaging of the brain and spine in these disorders plays an important role in diagnosis, as well as determining the extent of involvement and guiding surgical interventions. This article reviews the application of x-ray computed tomography and magnetic resonance imaging to these disorders, as well as that of newer, "functional" imaging techniques such as positron emission tomography, magnetic resonance perfusion imaging, and spectroscopy.
Semin Pediatr Neurol 13:48-62 © 2006 Elsevier Inc. All rights reserved.

KEYWORDS phakomatosis, neurocutaneous, neurofibromatosis, tuberous sclerosis, Sturge-Weber, von Hippel-Lindau, magnetic resonance imaging, spectroscopy, perfusion, computed tomography, brain, spine

The phakomatoses, also known as neurocutaneous syndromes, consists of a group of disorders that tend to develop hamartomatous malformations and neoplastic growths affecting the skin, the nervous system, and other organs. The more common phakomatoses include neurofibromatosis (NF), tuberous sclerosis (TS), Sturge-Weber disease (SW), and von Hippel-Lindau syndrome (VHL). Each of these has distinct clinical features and heterogeneous genetic profiles, yet shares the common characteristics of abnormal development of structures derived from ectodermal origin, such as in the central nervous system (CNS) and skin.[1] Of note, even though these are collectively called neurocutaneous syndromes, VHL lacks cutaneous findings, which also may not always be present in other disorders (eg, NF2). Among these, SW is considered sporadic disease because no genetic abnormality has been identified to date.

These syndromes are typically diagnosed clinically by a number of disease features, yet invariably in each there is a spectrum of disease manifestation and severity, sometimes making the diagnosis challenging. The genetic mutation has been identified in most of these entities, providing a better understanding of the underlying pathophysiology through a tumor suppressor mechanism,[1] as well as a more precise confirmatory test and potentially a means of prenatal diagnosis. Neuroimaging plays an integral part of the clinical evaluation by identifying lesions in the central nervous system. It not only aids the initial diagnosis but is also fundamental in delineating the extent of central nervous system involvement, in monitoring disease progression, and in providing an anatomic roadmap for potential surgical intervention.

This article reviews the imaging findings in the more common phakomatoses, including NF types 1 and 2, TS, SW, and VHL. The CNS manifestations on conventional computed tomography (CT) scans and magnetic resonance imaging (MRI) are discussed as well as the role of other imaging techniques such as diffusion-weighted images, magnetic resonance (MR) perfusion, MR spectroscopy, and the nuclear medicine positron-emission tomography (PET) and single photon emission computed tomography (SPECT) techniques. These newer imaging modalities may contribute to the understanding of the disease process by providing "physiologic" or "functional" information that complements the anatomic information present in conventional scans.

Neurofibromatosis

NF1

Type 1 neurofibromatosis, also called von Recklinghausen's disease, is the most common phakomatosis that occurs about 1 in 3,000 to 4,000.[2] It is transmitted as an autosomal dominant trait with the genetic defect localized to chromosome

*Russell H Morgan Department of Radiology and Radiological Science, Johns Hopkins University School of Medicine, Baltimore, MD; and
†Kennedy Krieger Institute, Baltimore, MD.
Address reprint requests to Doris D.M. Lin, MD, PhD, Department of Radiology, Phipps B100, Johns Hopkins University School of Medicine, 600 N Wolfe Street, Baltimore, MD 21287. E-mail: ddmlin@jhmi.edu
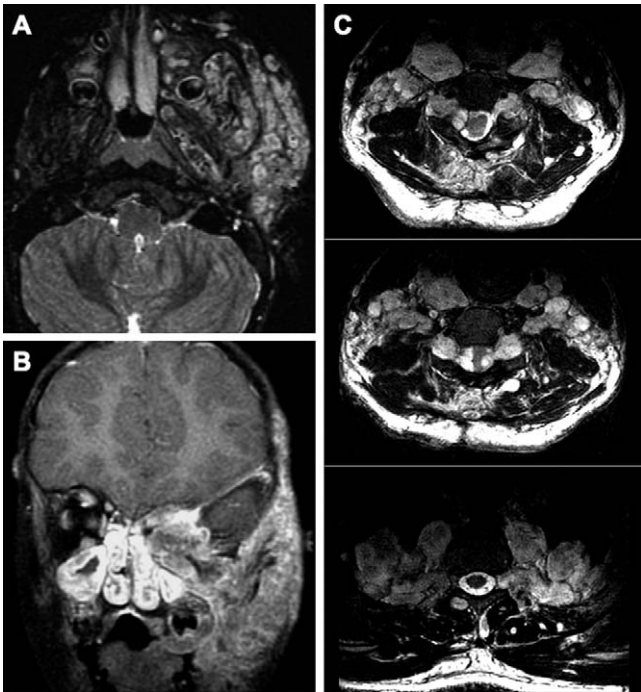
Figure 1 A 6-year-old boy with NF1 and left proptosis. (A) Axial T2 and (B) post-GdDTPA coronal T1-weighted images show extensive plexiform neurofibroma infiltrating the left face, periorbital soft tissue, masticator space, and parapharyngeal space. The mass is T2 bright with central dark areas and shows heterogeneous yet avid contrast enhancement. In this case, the plexiform neurofibroma also involves the retrobulbar compartment, and there is dysplasia of the left greater sphenoid wing. Both contributed to the marked distortion of the left orbit. (C) A 22-year-old man with NF1 and left arm pain. Three axial T2-weighted MR images through the lower cervical and upper thoracic spine show multiple plexiform neurofibromas involving the neural foramina, paraspinal, and prevertebral regions. The masses in the middle section fill the bilateral neural foramina and cause marked compression of the cord from both sides.

17q11.2 encoding neurofibromin. Neurofibromin is a tumor suppressor that regulates Ras-guanosine triphosphate activating protein and thereby controls cellular signal transduction.[3] Although it is hereditary, in 50% of the affected indi-
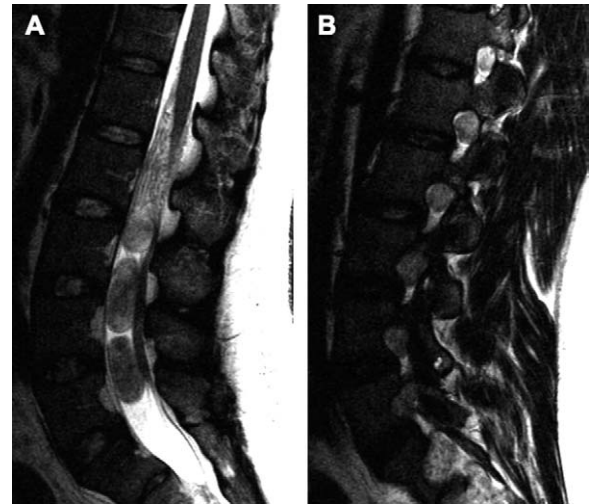

Figure 2 T2-weighted sagittal images of the lumbar spine showing multiple well-circumscribed neurofibromas (A) occupying the intradural extramedullary compartment of the spine and (B) expanding the neuroforamina.

viduals, NF1 occurs sporadically because of spontaneous mutation, and, in fact, it is the syndrome with the highest mutation rate. Affected individuals manifest with cutaneous "café au lait" spots, skinfold freckling, and neurofibromas. Lisch nodules, harmartomas of the iris, may also be found.

Neurofibromas are benign tumors arising from the nerve sheath and composed of a mixture of Schwann cells, perineural cells, and fibroblasts.[4] The neurofibromas can be nodular and discrete, or they can be diffuse, plexiform neurofibromas encasing and enlarging multiple nerve fascicles.[5] The plexiform neurofibroma is quite infiltrative and vascular and may occur in the deep spaces of the head and neck causing major disfiguration or in the paraspinal regions, resulting in nerve compression and neurologic deficits (Fig 1). On MRI, these masses are typically T1 hypointense and T2 hyperintense, with a variable contrast-enhancement pattern.[6] There is estimated to be a 10% risk of development of malignant peripheral nerve sheath tumors, often of the plexiform type, in NF1
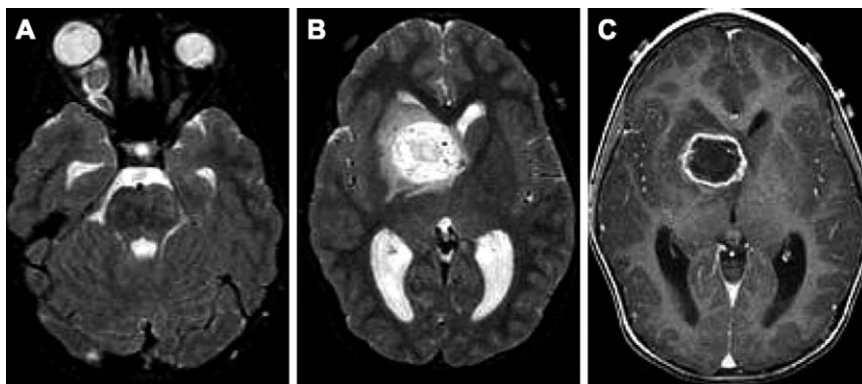

Figure 3 A 7-year-old girl with NF1. (A) Axial T2-weighted image shows right optic nerve glioma with proptosis. (B) Axial T2 and (C) post-GdDTPA axial T1-weighted images show a right basal ganglia mass with rim enhancement, central necrosis, and associated edema and mass effect on the ventricles resulting in mild obstructive hydrocephalus. Surgical pathology revealed a low-grade astrocytoma.
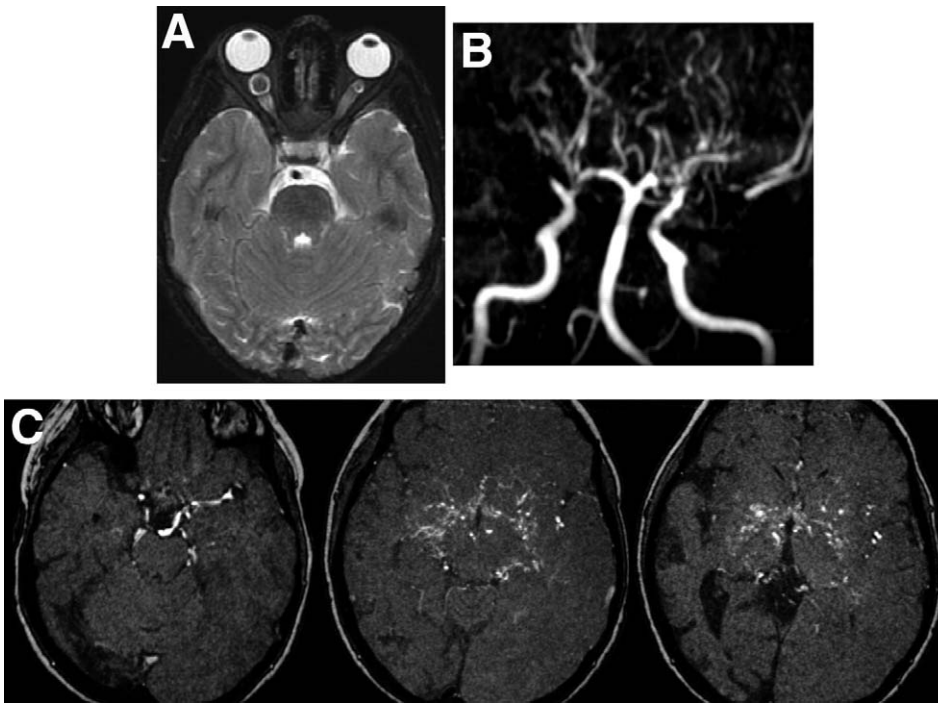
Figure 4 A boy with NF1. (A) An axial T2-weighted image shows bilateral optic nerve gliomas, which are larger on the right. The distal internal carotid artery flow voids are not well seen. (B) MR angiography of the circle of Willis shows stenosis of the distal internal carotid arteries and complete occlusion at the termini, with no flow in the right middle cerebral artery and severe narrowing of the left middle cerebral artery. Many collateralized lenticulostriate vessels are seen instead. (C) Axial time-of-flight gradient-echo source images of the MR angiogram again show the moya-moya pattern of collateral vessels around the brainstem and in the bilateral basal ganglia regions.

patients.[7] Imaging findings of irregular contour and heterogeneous enhancement are suggestive of invasive nature; however, some of the malignant peripheral nerve sheath tumors have a similar appearance to the benign ones. A few studies suggested that F18-deoxyglucose positron-emission tomography (FDG-PET) may be useful in distinguishing the malignant from benign peripheral nerve sheath tumors.[8-10] Multiple spinal neurofibromas tend to occur in NF1 patients as tumors in the intradural extramedullary, extradural, or mixed compartments. They have a characteristic feature of a dumbbell shape, expanding the neural foramina (Fig 2) and often exhibiting central dark signal on T2-weighted images reflecting dense collagen formation on histopathology.

Intracranially, NF1 patients have the tendency of developing neoplasms including optic pathway gliomas that are typically of the juvenile pilocytic astrocytoma histology (Fig 3A)

as well as astrocytomas in other brain regions (Fig 3B and C). The incidence of CNS tumors in NF1 is about 1% to 5%.[11] Among these, the optic nerve gliomas are most common. They are slow-growing tumors that directly infiltrate and enlarge the optic nerve and can involve any portion of the optic pathway including the intraorbital optic nerves, chiasm, optic tracts, lateral geniculate bodies, and optic radiations. The intraorbital and chiasmal optic gliomas may enhance with gadolinium-diethylenetriamine penta-acetic acid (GdDTPA) either avidly or mildly, whereas the extension along the lateral geniculate, optic tracts, and radiations typically shows expansion and T2 prolongation without contrast enhancement. Visual acuity usually declines slowly and is the most common clinical presentation.[12]

A number of nonneoplastic abnormalities are often encountered in NF1. Mesenchymal dysplasia associated with

Figure 5 A 20-year-old woman with NF1. (A) A sagittal T2-weighted image shows widening of the thoracic spinal canal with scalloping of the posterior vertebral bodies caused by dural ectasia. (B) Sagittal and (C) axial T2-weighted images show outpouching of the meninges, smooth pressure erosion of the posterior vertebral body, and widening of the left neural foramen because of a large lateral meningocele.
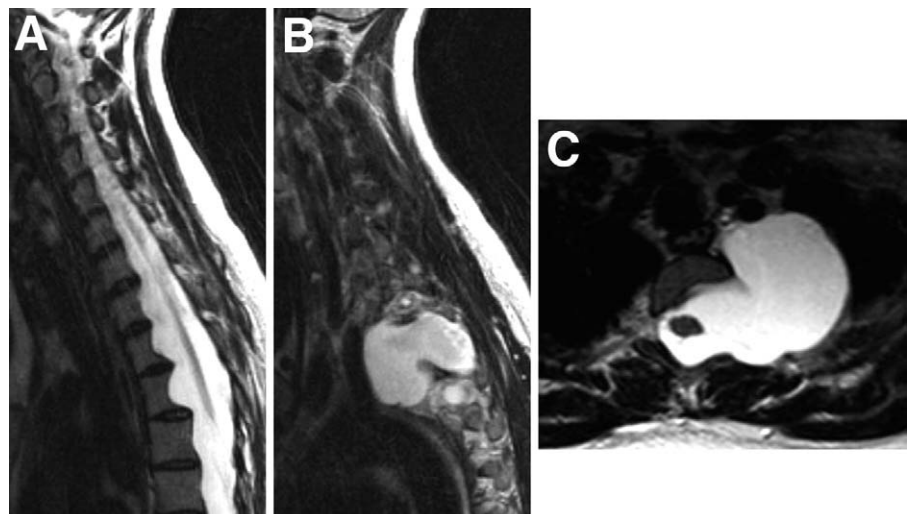
Figure 6 NF1. (A) Axial and (B) coronal CT images of the orbit show a defect in the right greater wing of the sphenoid bone, resulting in asymmetric herniation of the right temporal lobe causing proptosis of the right eye. Note also an enlarged left optic nerve because of an optic nerve glioma. (C) A surface-rendered 3-dimensional reconstruction of the skull shows and empty socket appearance on the right side and an open bony defect. (Color version of figure is available online.)
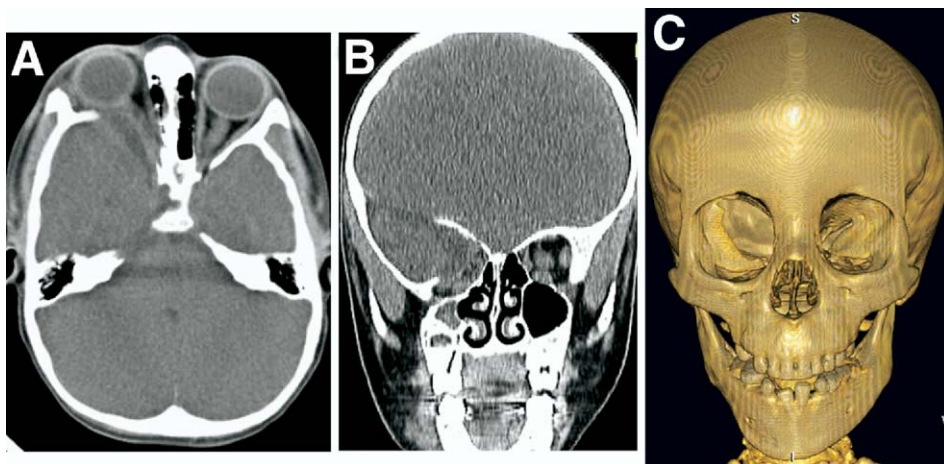
NF1 leads to defective connective tissue, ranging from bony abnormalities such as sphenoid wing dysplasia, vascular abnormalities such as intracranial aneurysm, stenosis, and moyamoya syndrome (Fig 4), to dural dysplasia. Scalloping of the posterior vertebrae may be seen with intraspinal tumors but more typically as an isolated finding related to dural ectasia. Weakness or defect of the meninges in the spine gives rise to characteristic arachnoid cysts or lateral meningoceles, which most commonly occur in the thoracic region (Fig 5). Sphenoid wing dysplasia occurs uncommonly, in about 1% of cases. This can result in pulsatile exophthalmos related to transmission of cerebrospinal fluid pulsations through the bony defect and herniation of the temporal lobe (Fig 6).

With the advent of MRI, it has been found that 60% to 90% of NF1 individuals, without any neurologic symptoms, have lesions on long T2-weighted sequences.[13-15] These lesions have been coined the name "unidentified bright objects" (UBOs) and are typically found bilaterally in the dentate nuclei of the cerebellum, brainstem, basal ganglia, and thalami in a symmetric or asymmetric fashion (Fig 7). Atypical location may also be found such as in the cerebral white matter. They are not associated with any mass effect or enhancement. On pathology based on autopsy cases, these lesions correspond to vacuolar changes in the myelin sheath.[16] It is of interest that they often decrease in number and size between 7 and 12 years of age, after which they gradually increase and then decrease again. The evolution may also shift in location.[17] It has been noted that UBOs are found in only 29% of NF1 individuals older than 31 years. Even though these lesions do not cause neurologic symptoms, they have been correlated with learning disabilities.[18-20] At times, UBOs may have an atypical appearance (such as mass-like, associated with apparent mass effect) or location that makes it difficult to distinguish from an astrocytoma. A UBO should never enhance with Gd, yet the typical low-grade glioma (astrocytoma) also does not show any enhancement. In such cases, 1H-MR spectroscopy may be helpful. It has generally been found that the metabolic profile in these UBOs is not very different from that of a normal brain, suggesting that the
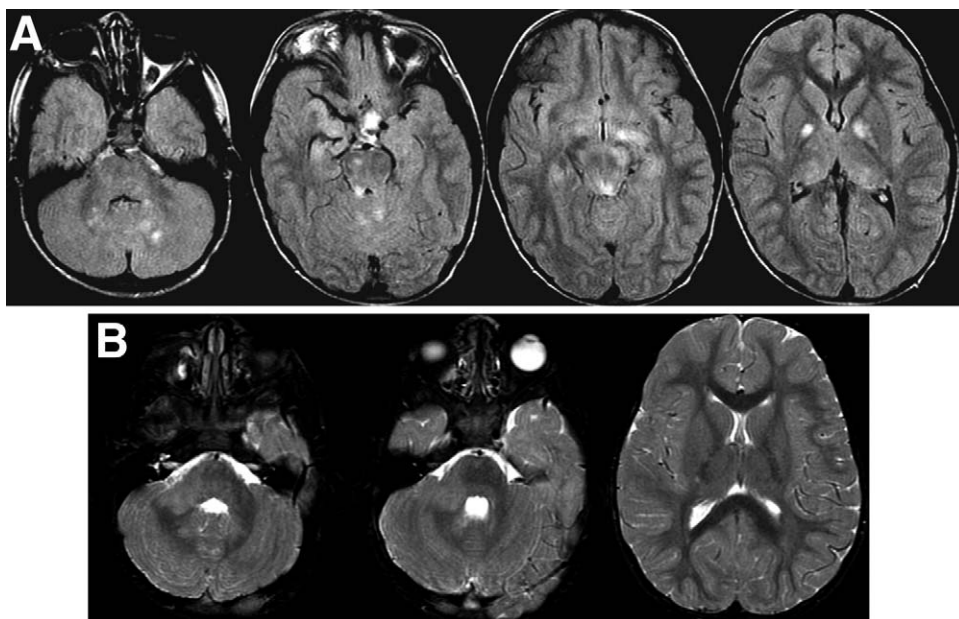

Figure 7 Two cases with NF1. (A) FLAIR images show typical distribution of bright lesions (UBOs) in the cerebellar dentate, pons, cerebellar peduncles, midbrain, globus pallidi and thalami. (B) UBO in a 22-month-old girl: T2-weighted images showing asymmetrically located, mass-like lesion in the right middle cerebellar peduncle, which appears somewhat expanded.
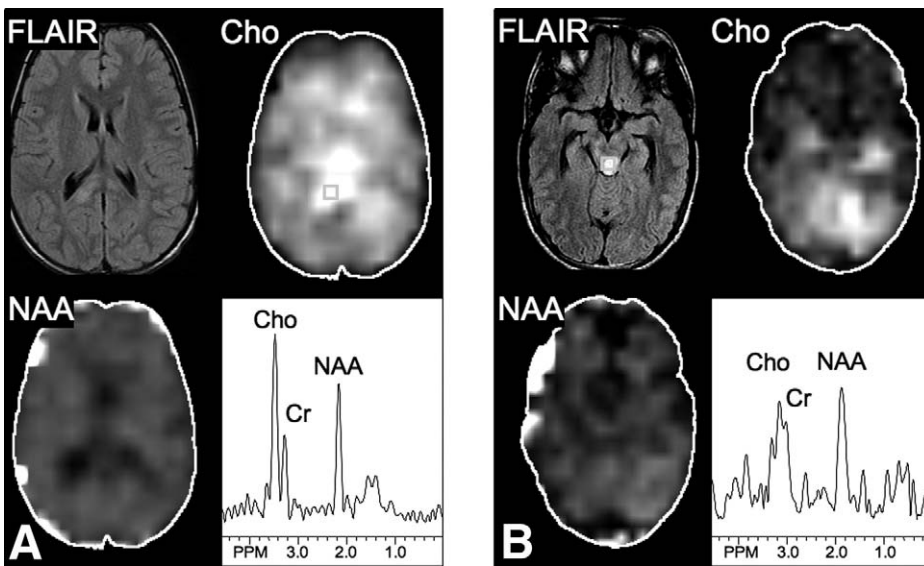
Figure 8 Brain lesions and associated proton MR spectroscopic imaging findings in patients with NF1. (A) Glioma in the splenium of the corpus callosum shows increased levels of Choline (Cho) consistent with a neoplasm. (B) UBO in the midbrain just anterior to the quadrigeminal plate shows near normal metabolite levels, in particular with no evidence of increased Cho signal.

"vacuolar changes" simply reflect areas of edema or holes (Fig 8).

NF2

In contrast to NF1, there is minimal skin manifestation in individuals affected by NF2, and the prevalence of NF2 is much lower, about 1 in 40,000. NF2 is characterized by bilateral vestibular schwannomas (Fig 9),[21,22] also known as central form of neurofibromatosis or vestibular schwannoma neurofibromatosis. Diagnosis can be made on the basis of (a) bilateral vestibular masses, or (b) a positive family history with either unilateral vestibular mass, or any 2 of meningiomas, gliomas, schwannomas, and congenital catatacts.[23,24] The genetic defect has been localized to chromosome 22q12.2.[25,26] In 50% of the cases, however, the disease occurs as a result of spontaneous mutation.

Because of the prevalence of multiple intracranial and intraspinal neoplasms, NF2 is also known as Multiple Inherited Schwannomas, Meningiomas, and Ependymomas Syndrome.[27] These are readily identified on contrast-enhanced MRI.[6] Schwannomas can be innumerable, showing as enhancing lesions involving multiple cranial nerves as well as within the intradural compartment along the spinal nerve roots (Fig 10) and in the peripheral nerve sheath within the paraspinal regions (Fig 11A). Intraspinal schwannomas tend to grow as large dumbbell-shaped masses expanding the neural foramina, most commonly intradural extramedullary in location but may be located extradurally or occupy both compartments (Fig 11). They are characteristically bright on T2-weighted images, with avid and homogeneous contrast enhancement (Fig 12) and at times a tendency of becoming cystic. In contradistinction to neurofibromas, they do not have a malignant potential. Schwannomas displace but do not infiltrate the adjacent nerve roots; therefore, surgical resection is possible. Multiple meningiomas often occur intracranially in the extra-axial compartment (Fig 13) and occasionally in the intraventricular location (Fig 14). They can also be found in the spine as extramedullary masses. On a CT scan, they are slightly hyperdense, dural based, and may have associated hyperostosis of the adjacent bone. On MRI, they are typically isointense to gray matter on both T1- and T2-weighted images, with avid and homogeneous contrast enhancement. In the general population, meningioma repre-

Figure 9 A 21-year-old man with NF2 presenting with right ear deafness and right facial paralysis. (A) Axial and (B) coronal T1-weighted MR images post GdDTPA show bilateral vestibular schwannomas, which are larger on the right side. The right-sided tumor has a large cerebellopontine angle component, and both masses extend into the internal auditory canals causing expansion.
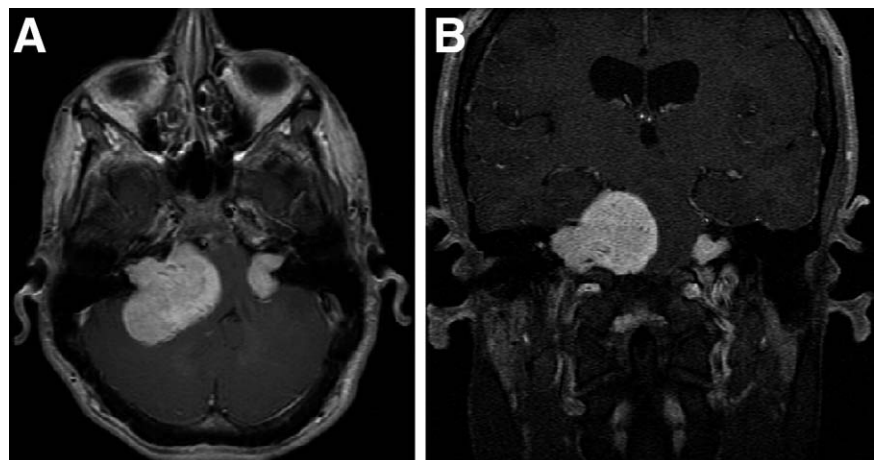
Figure 10 An 18-year-old female with NF2. Post-GdDTPA sagittal T1 weighed image of the (A) cervicothoracic and (B) lumbar spine show innumerable enhancing schwannomas along the surface of the cord and nerve roots of the cauda equina.

sents a common extra-axial neoplasm most often encountered in older females, with its growth under the influence of estrogen. When meningioma occurs in a child, the association of NF2 should be considered. Finally, in NF2, there is a tendency of developing multiple ependymomas that typically present as intramedullary enhancing masses in the spine (Fig 15) of the cellular histological type.[28,29] They are well-circumscribed masses centrally located in the cord, usually exhibiting T1 isointensity and T2 hyperintensity relative to the adjacent parenchyma, and are associated with strong contrast enhancement.

TS

Also know as Bourneville disease, TS is characterized by a triad of seizure, mental retardation, and facial angiofibroma (adenoma sebaceum being a common misnomer). Seizures affect more than 75% of TS patients, and there is also a high rate of learning difficulties, cognitive impairment, and behavorial problems.[30-32] Similar to other phakomatoses, TS man-

ifests as hamartomatous growths in multiple organ systems including skin, heart, eye, kidneys, and lungs, in addition to involvement of the central nervous system. The prevalence is about 1 in 6,000 to 10,000 births, with 60% to 70% cases of sporadic occurrence.[33] It is an inherited disorder with an autosomal dominant trait. Chromosomal abnormality has been localized to 9q34, encoding *TSC1* or hamartin,[34] and to 16p13.3, encoding *TSC2* or tuberin.[35] Both gene products form a cytoplasmic protein heteromeric complex and act as tumor suppressors affecting the regulation of cellular growth, adhesion, and migration.[36,37]

Intracranial findings clearly show malformations as a result of perturbed proliferation, histogenesis, and migration of neuronal and glial cells.[38,39] The hamartomatous lesions can be found anywhere from the ependymal surface to the cortex, and are composed of abnormal giant or balloon cells that may exhibit features of astrocytes, neuronal cells, or intermediate forms. These lesions include subependymal nodules, cortical and subcortical tubers, and subependymal giant-cell astrocytoma.[40,41] All 3 forms are considered the major features in the revised diagnostic criteria from the Tuberous Sclerosis Complex Consensus Conference in 1998,[42] making imaging an important part of establishing the clinical diagnosis. In the revised criteria, 2 major features or 1 major plus 2 minor features are diagnostic; fulfilling 1 major and 1 minor feature is considered probable TS. In addition to these typical findings, white-matter signal abnormalities reflecting "migration lines" can be seen as bands of myelination defect or gliosis.[43,44]

The MR appearance of these major lesions varies with age.[38,45] In the perinatal to early infancy periods, they are best seen as T1 bright lesions, including the white-matter lines along the trail of radial glia and migrating neurons (Fig 16). Later in life, the subependymal nodules are often calcified and may be depicted on T1-weighted images as isointensity to mild hyperintensity and mild T2 hypointensity. Cortical and subcortical tubers as well as white-matter migration lines are best seen on long TR sequences, particularly fluid-attenuated inversion recovery (FLAIR).

Subependymal nodules represent disorganized glial and neuronal elements and can be found lining the ependymal margin and protruding into the ventricular system, yielding an appearance of "candle guttering" (Fig 17). Even though these nodules show signal intensity similar to gray matter,

Figure 11 NF2. Post-GdDTPA axial T1-weighted images of the upper thoracic region show (A) bilateral large extradural spinal schwannomas. Note multiple enhancing schwannomas are also present in the posterior paraspinal regions bilaterally. (B) In addition, there are enhancing masses within the spinal canal in the intradural compartment, compressing the cord at this level.
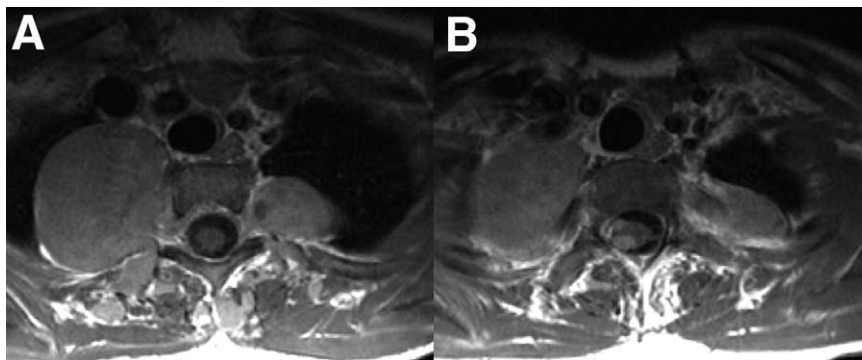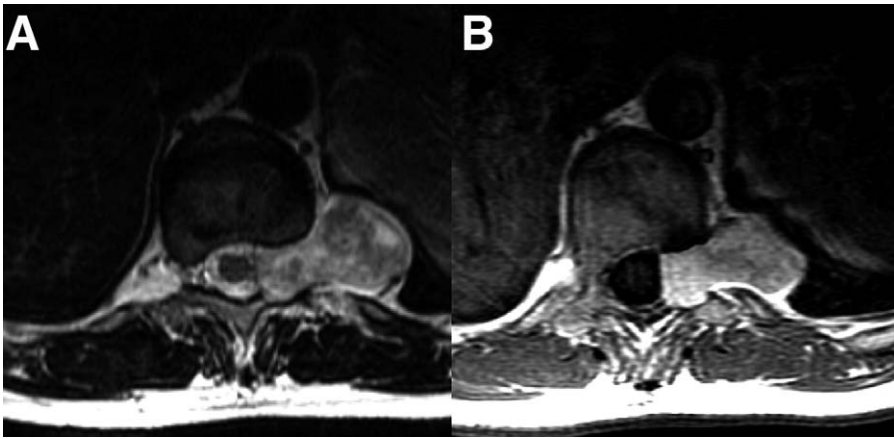
Figure 12 NF2 patient with radioculopathy. (A) Axial T2-weighted and (B) axial post-GdDTPA T1-weighted images show a dumbbell-shaped T2 hyperintense mass with intense enhancement, characteristic of a schwannoma. In this case, the mass is extradural in location, expanding the left neural foramen and causing flattening of the thecal sac on the left side.
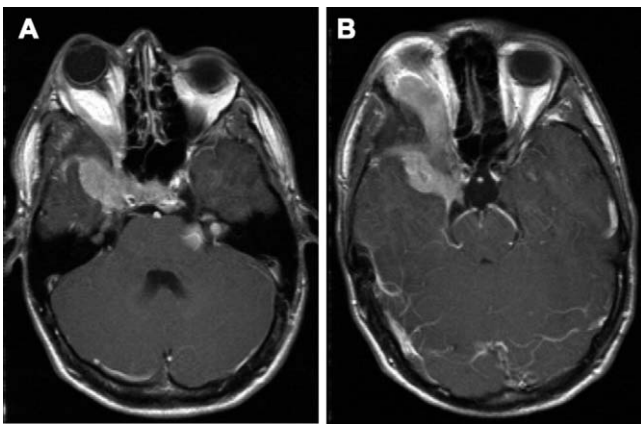

Figure 13 NF2 patient with (A) bilateral seventh and eighth nerve complex masses representing vestibular schwannomas and a lobular extra-axial enhancing mass reflecting a meningioma along the right greater wing of the sphenoid that extends intraorbitally resulting in a proptotic right eye.

they are slightly hyperintense on FLAIR, probably reflecting increased water content.[46] Not infrequently, these nodules calcify, best seen on CT scans, but also found on MRI, causing dephasing or loss of signal intensity, particularly on susceptibility weighted images. Some of these nodules enhance
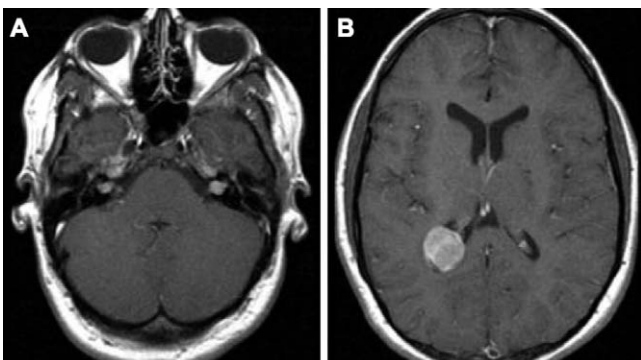
with GdDTPA without indicating any increased neoplastic potential. There is a 5% to 14% estimated risk of developing intracranial neoplasm–giant-cell astrocytoma (Fig 18) from the subependymal nodule that is located at the foramen of Monro, often resulting in obstructive hydrocephalus. Histologically, this again represents a mixture of varied glioneuronal phenotypes with dysplastic-appearing giant cells.[4] It is a discrete, low-grade neoplasm of World Health Organization class I amenable to surgical resection. Subcortical and cortical tubers similarly represent a disorganized cluster of glioneuronal elements, with variable degrees of differentiation, and have a strong association with epilepsy, particularly manifesting as infantile spasms and generalized tonic-clonic seizures. They typically show areas of hyperintensity on long TR sequences located in the subcortical white matter, with-
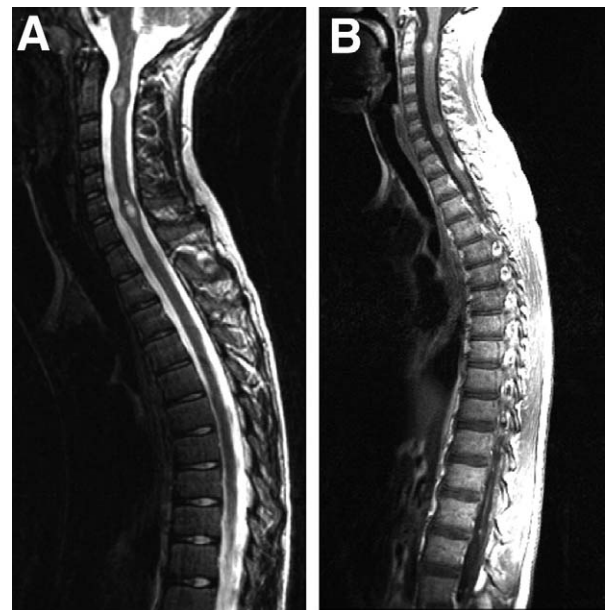

Figure 14 A 14-year-old girl with NF2 shows (A) bilateral intracanalicular vestibular schwannomas and (B) an intensely enhancing intraventricular meningioma in the right lateral ventricular trigone.

Figure 15 NF2. (A) Sagittal T2 and (B) post-GdDTPA sagittal T1-weighted images of the cervical and thoracic spine show multiple intramedullary masses, most concentrated in the cervical region, reflecting multiple ependymomas. A number of additional enhancing lesions along the surface of the cord and cauda equina are most likely intradural schwannomas.

Figure 16 TS. A 5-day-old male infant who had multiple cardiac masses previously detected in utero. (A) An axial T1-weighted image reveals a large soft-tissue mass abutting the left ventricle and displacing the heart to the right side. (B) Axial T1-weighted images show multiple linear hyperintense lesions along the subcortical white matter reflecting cortical/subcortical tubers as well as small round lesions along the ependymal surface representing subependymal nodules. Note that a more prominent lesion near the right foramen of Monro in the middle section is suggestive of a subependymal giant-cell astrocytoma. Some of the white matter linear lines (eg, in the right frontal and left parietal regions) are elongated and approximating the ventricles, characteristic of migration lines.
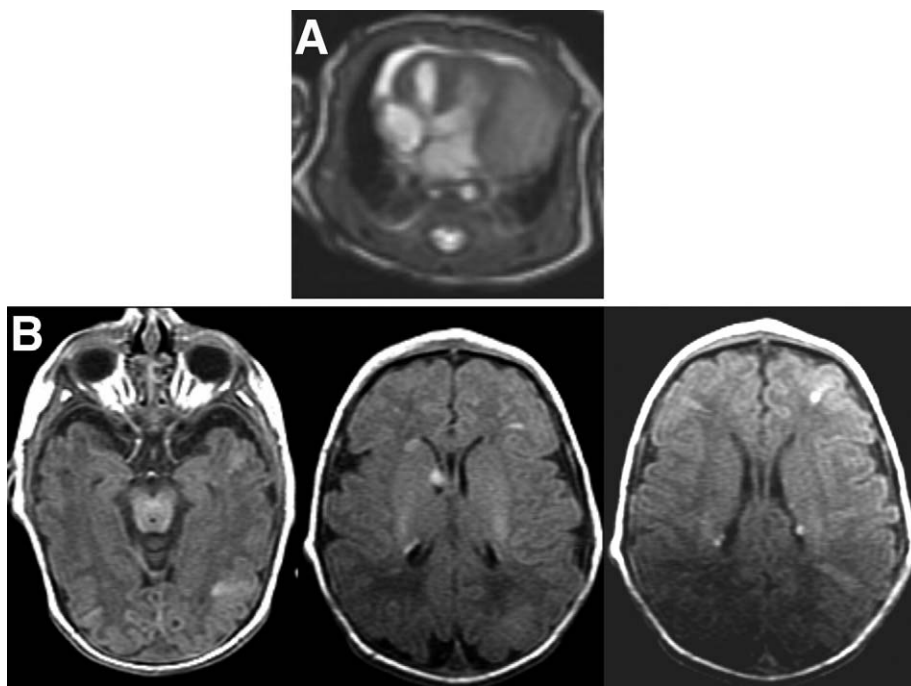
out associated mass effect or enhancement.[38,40,44] They may also calcify (Fig 19). The associated white-matter signal abnormality at times shows a linear or wedge-shaped track extending from the ventricular surface. This is thought to

represent the trail of radial glial cells during the migration and proliferation process.

Variable forms of congenital anomaly have been reported in association with TS, ranging from transmantle cortical dysplasia and corpus callosum dysgenesis to findings of schizencephaly and hemimegalencephaly.[38,47] Infratentorial abnormalities can also be found (Fig 20), including cerebellar folia or nodular white-matter calcifications, cerebellar hemisphere and vermis agenesis or hypoplasia, enlargement of the cerebellar hemisphere, and brainstem and fourth ventricle subependymal nodules and tubers.[39]

Proton MR spectroscopy of cortical tubers and subependymal nodules show decreased N-acetylaspartate/creatine (NAA/Cr) and increased myoinositol/Cr ratios. This pattern was thought to reflect expression of immature neurons and glia or gliosis as a result of disturbed cell migration and differentiation in TS.[48,49] In addition to these similar findings, another study correlated the detection of lactate to the regions of epileptic foci on electroencephalography (EEG) in 6 patients.[50] On diffusion-weighted imaging, cortical tubers show significantly increased apparent diffusion coefficient (ADC) values compared with normal controls.[51,52] Furthermore, in a study of 4 TS patients who had unifocal interictal spikes on EEG and magneticoencephalography, ADC was significantly higher in the 4 epileptogenic tubers than 18 nonepileptogenic ones, which in turn showed significantly higher ADC compared with that in a normal-appearing cortex.[53] These findings are yet to be confirmed in a larger series (preferably with correlation of surgical outcomes). However, it would be of significant value if noninvasive imaging techniques can depict the primary epileptogenic focus in those patients being considered for surgical seizure management.

Perfusion-weighted MR images in a child of multiple calcified tubers in the subcortical white matter shows decreased
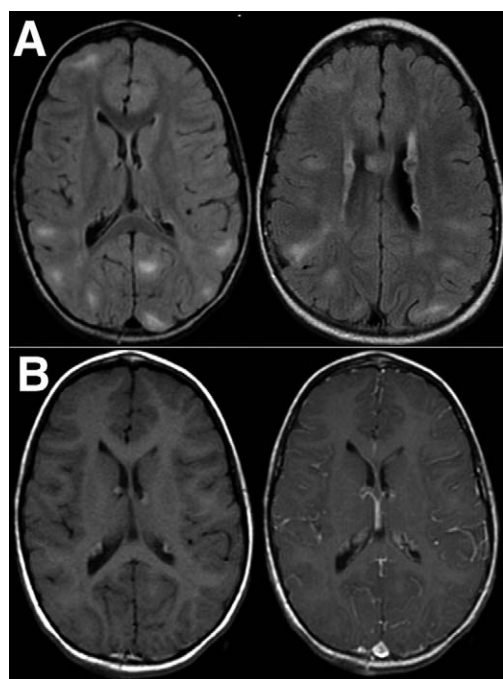

Figure 17 A 7-year-old girl with TS. (A) FLAIR images show multiple hyperintense cortical and subcortical tubers. In addition, several small subependymal hamartomas are present, showing slight FLAIR and T2 hypointensity likely reflecting calcification. (B) Axial T1-weighted images before and after GdDTPA show that the subependymal hamartomas are T1 hyperintense without additional enhancement, which is also consistent with calcific deposits.
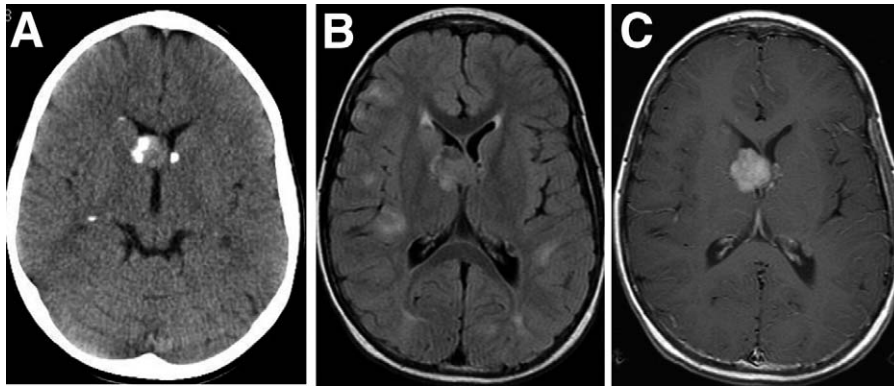
Figure 18 TS. (A) Noncontrast-enhanced head CT scan shows a partially calcified intraventricular mass near the foramen of Monro representing a subependymal giant-cell astrocytoma. Additional punctate calcifications reflect calcified subependymal nodules. (B) FLAIR image shows multiple cortical and subcortical tubers to best advantage. (C) A post-GdDTPA T1-weighted axial image shows avid contrast enhancement in the foramen of Monro giant-cell astrocytoma. There is no hydrocephalus in this case.

overall perfusion compared with adjacent normal-appearing white matter, and in some of the core of the calcified tubers, there is virtually absent perfusion (Fig 21). Perfusion deficit in the tubers is confirmed in multiple prior radionuclide SPECT and PET studies.[54,55] A more specific radionuclide agent, alpha-[11C]methyl-L-tryptophan ([11C]AMT) assessing serotonin uptake was found to be useful in discriminating the epileptogenic from nonepileptogenic foci in TS patients. Although multiple tubers show decreased glucose metabolism on FDG-PET, there was a differential pattern of [11C]AMT uptake; the tubers with increased uptake had a high correlation with the epileptogenic foci detected on ictal EEG.[56] Moreover, resection of the high [11C]AMT-uptake tubers allowed achievement of seizure-free outcome in children with TS, suggesting that AMT-PET can provide an excellent test for presurgical patient selection and seizure localization.[57]

SW

SW, also known as trigemino-encephalo-angiomatosis, is characterized by a cutaneous port-wine stain typically in the ophthalmic division of the trigeminal nerve distribution and intracranial leptomeningeal angiomatosis ipsilaterally.[58] There are often ocular abnormalities as well, including con-

genital glaucoma and choroidal angioma, affecting the same side as the cutaneous capillary angioma. SW is relatively rare, occurring in about 1 in 40,000. Although there are familial cases, thus far no genetic link has been identified, and SW is thought to occur sporadically.[59,60] Common neurologic manifestations in affected individuals include seizure, developmental delay, cognitive impairment, visual field defect, headache, and stroke-like symptoms.

The presence of facial port-wine stain at birth raises the suspicion of the diagnosis, but port-wine stain itself is a common cutaneous finding, and only 8% of individuals with port-wine stain have intracranial involvement that is characteristic of SW.[61] Clinically, the expression of SW is variable. In 1992, Roach[62] provided a classification scheme based on the varying degrees of involvement as follows: type 1, classic and the most common form, manifesting both facial and leptomeningeal angiomatosis with or without glaucoma; type 2, facial angioma and possible glaucoma, without intracranial involvement; and type 3, leptomeningeal angioma but no facial angioma or ocular manifestation of disease.

Conventional MRI and CT scans have been useful in aiding the diagnosis of SW and showing the extent of intracranial involvement.[63] A CT scan best shows the classic tram-track calcification of the cortex (Fig 22A), whereas MRI with contrast provides the most sensitive means of depicting lepto-
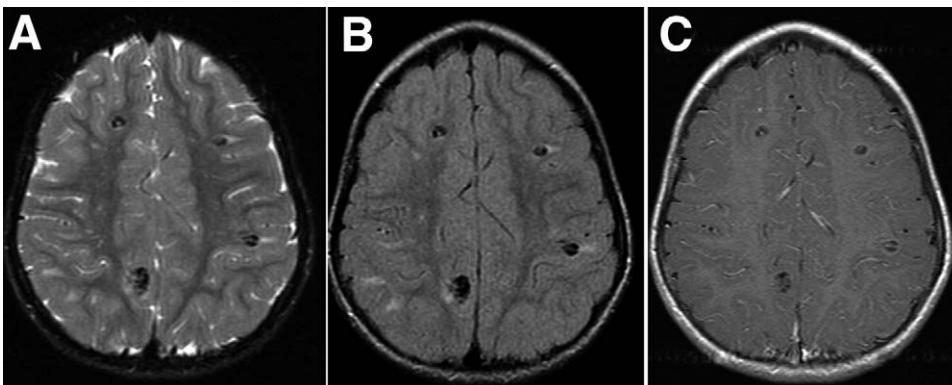

Figure 19 A 7-year-old girl with TS presenting with infantile spasm and autism. (A) Axial T2, (B) axial FLAIR, and (C) post-GdDTPA axial T1-weighted images show multiple calcified subcortical tubers that appear dark because of the dephasing effect. Additional noncalcified tubers can be seen in (A) and (B) in the subcortical white matter and centrum semiovale. There is no associated edema, mass effect, or enhancement.
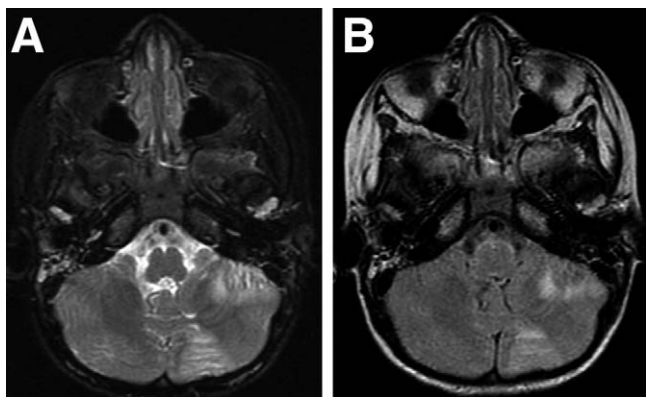
Figure 20   Wedge-shaped cerebellar hamartomas shown on (A) T2 and (B) FLAIR images in a 7-year-old girl with TS.

Figure 22   A 15-year-old boy with SW. (A) A noncontrast-enhanced CT scan shows tram-track calcification of the left parietal-occipital cortex. (B) A post-GdDTPA T1-weighted MR image shows leptomeningeal enhancement in the similar region.

meningeal enhancement that is considered the hallmark of the disease (Fig 22B), in addition to cortical atrophy.[64,65] The leptomeningeal angiomatosis represents embryonic venous plexus that is normally present during 4 to 8 weeks of fetal life. The failure of regression and lack of development of normal cortical veins results in ineffective venous drainage, venous stasis and hypertension, and subsequent ischemia of the underlying brain.[58] In the early stage of disease, involvement is most frequently seen in the parietal and occipital lobes, sometimes followed by temporal and frontal lobes resulting in hemiatrophy of the brain. Bilateral involvement occurs in about 15% of cases.[66] Post–contrast T1-weighted FLAIR images have been advocated to better depict leptomeningeal disease.[67] It was found that these images show leptomeingeal enhancement with greater conspicuity compared with the conventional post–contrast T1-weighted spin-echo images, probably by suppressing the vascular signals (Fig 23). In addition to pial angiomatosis that shows enhancement, there are frequently choroidal glomi and transmedullary venous angiomas that likely form a collateral venous drainage pathway because the cortical venous system is dysplastic. These transmedullary veins and surface angio-
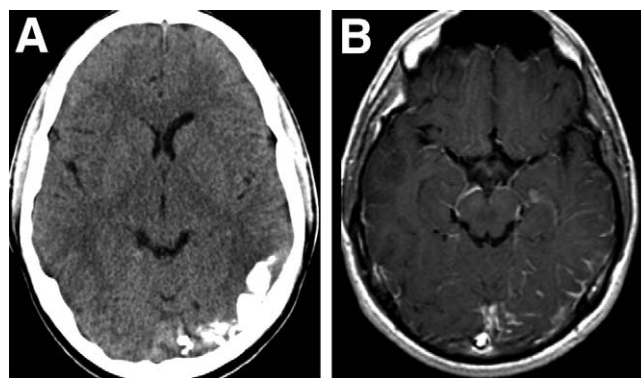
matosis can be exquisitely depicted using long echo time susceptibility weighted gradient-echo MRI or high-resolution MR venography (Fig 24). This sequence uses the intrinsic contrast of venous blood that is rich in deoxyhemoglobin that appears dark in the background of the brain parenchyma because of T2* dephasing effect.[68,69] By use of this particular sequence, there has been a report of earlier detection of evolving leptomeningeal angiomatosis in an infant with SW before it is evident on post–contrast T1-weighted images.[70]

Nuclear medicine studies including PET and SPECT have traditionally been used to assess functional hypoperfusion in SW as a result of anomalous venous development. Cerebral perfusion imaging using Technetium-99m hexamethylpropyleneamineoxime SPECT have shown hypoperfusion in the area of vascular malformation that is at times more extensive compared with abnormalities depicted on CT scans and MRI.[71,72] It is suggested that functional measures may be more sensitive for the early diagnosis of the disease because several cases showed that the perfusion (estimated by using SPECT) and metabolism (assessed by using FDG-SPECT) alterations were evident before the development of structural

Figure 21   Dynamic contrast-enhanced susceptibility weighted MR perfusion in tuberous sclerosis. Multiple calcified subcortical tubers are best depicted on susceptibility weighted (T2*-weighted gradient echo) sequence, whereas non-calcified tubers are seen on FLAIR. The right-hand panel of signal intensity versus time plot shows decreased perfusion within the subcortical tubers (white box and plot) or nearly absent perfusion (yellow box and plot). (Color version of figure is available online.)
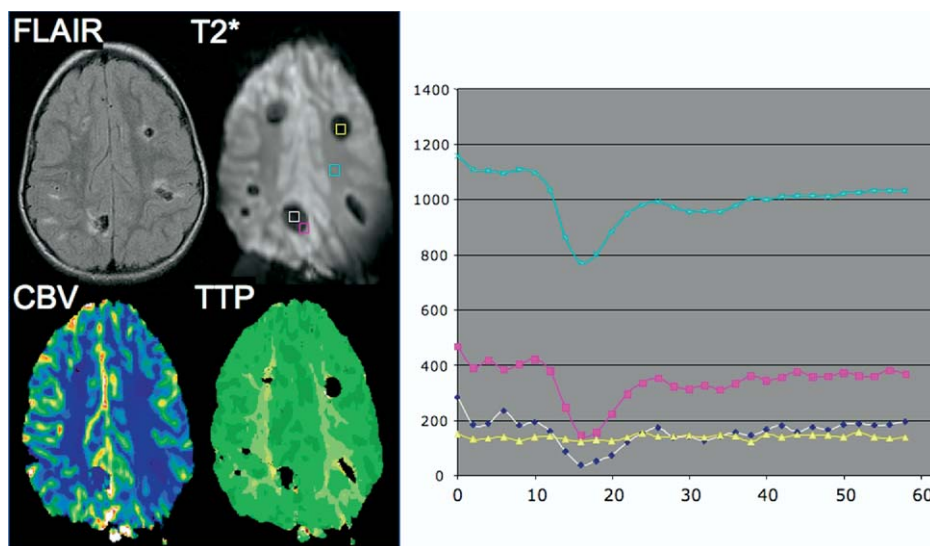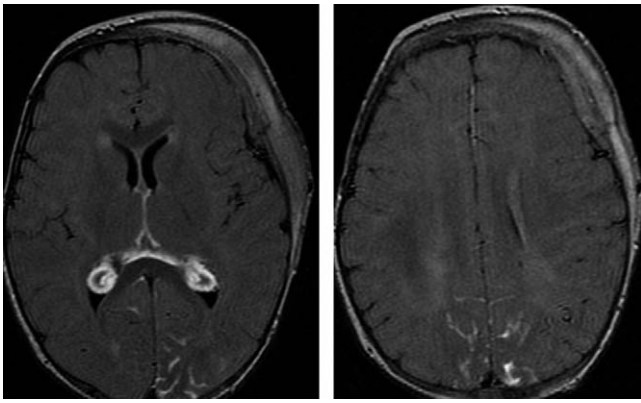
Figure 23   Post-GdDTPA FLAIR images in a 2-year-old boy with SW show enlarged choroid glomi on both sides as well as leptomeningeal enhancement in the bilateral occipital regions. Also noted in this case is the left frontal osseous thickening.

Figure 24   Susceptibility weighted image, or 3-dimensional blood oxygen level dependent (BOLD) venography, shows abnomal leptomeningeal angioma along the right temporal lobe in a 17-year-old male with SW. This sequence prominently depicts numerous small cortical and deep veins in the brain.

abnormalities.[73] Reductions in perfusion and glucose metabolism also corresponded to the patterns of neurologic deterioration in these patients.[74] In addition, a relationship was shown between seizure frequency, lifetime number of seizures, and hemispheric area of asymmetric cortical metabolism. More recently, perfusion deficits in SW have also been examined by using dynamic contrast MR perfusion technique (Fig 25), similar to that typically used in evaluating acute cerebral infarction.[75] This allows a simple yet comprehensive examination in the same MR study that is used to delineate structural abnormality in SW patients, to avoid the risk of ionizing radiation, and to provide information on abnormalities caused by either the arterial or venous phase.

Proton MR spectroscopy depicts abnormalities of metabolites, providing an independent functional assessment of these patients. Typically in older SW children corresponding to the region of cerebral atrophy, a decreased NAA is identi-
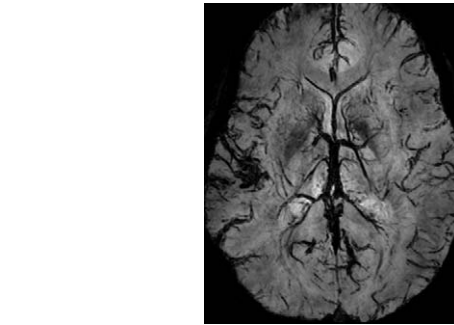
fied suggesting neuronal dysfunction or loss (Fig 26).[56,76] At the early stage of disease and (eg, during the first few years of life), however, the NAA level has been found to be normal, whereas choline is slightly elevated, perhaps reflecting abnormal development or myelination.[75]

VHL

Also known as retinocerebellar angiomatosis, VHL is inherited as an autosomal dominant trait with variable penetrance.[77,78] The incidence is about 1 in 36,000.[79] The abnormality has been localized to chromosome 3p25-p26,[80] which encodes a tumor suppressor as a regulator of hypoxia-inducible genes.[81] Although most affected individuals inherit the abnormality, 20% are caused by a spontaneous mutation. The symptoms usually manifest in the second to third decade of life. In VHL, patients present with congenital capillary angiomatous harmartomas in the CNS, including cerebellar
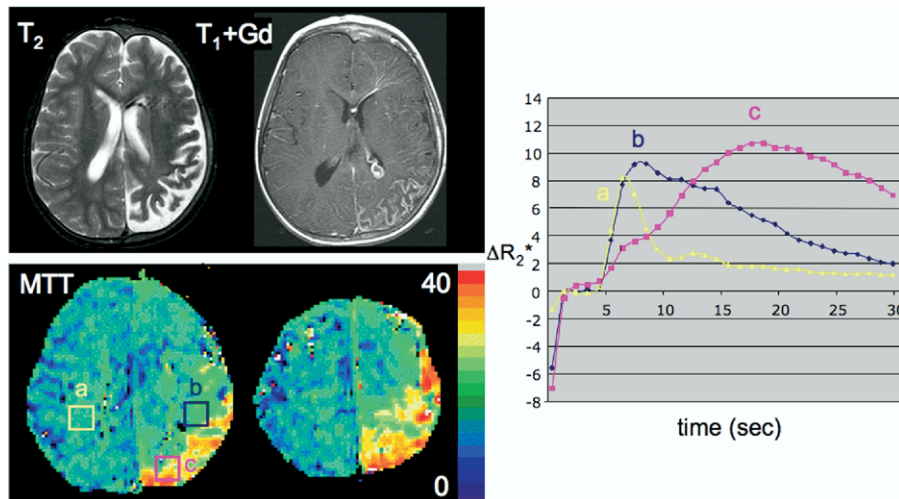
Figure 25   A dynamic contrast enhanced susceptibility weighted MR perfusion in a 4-year-old girl with SW. Corresponding to marked cortcial atrophy and leptomeningeal angiomatosis in the left parietal lobe, there is marked hypoperfusion (shown as prolonged mean transit time, MTT) and venous stasis (magenta box and plot). The MTT scale is in seconds (range 0 to 40), with increasing MTT representing slower flow. In the y-axis, delta R2* represents the change of the inverse transverse ralaxation time T2*. (Color version of figure is available online.)

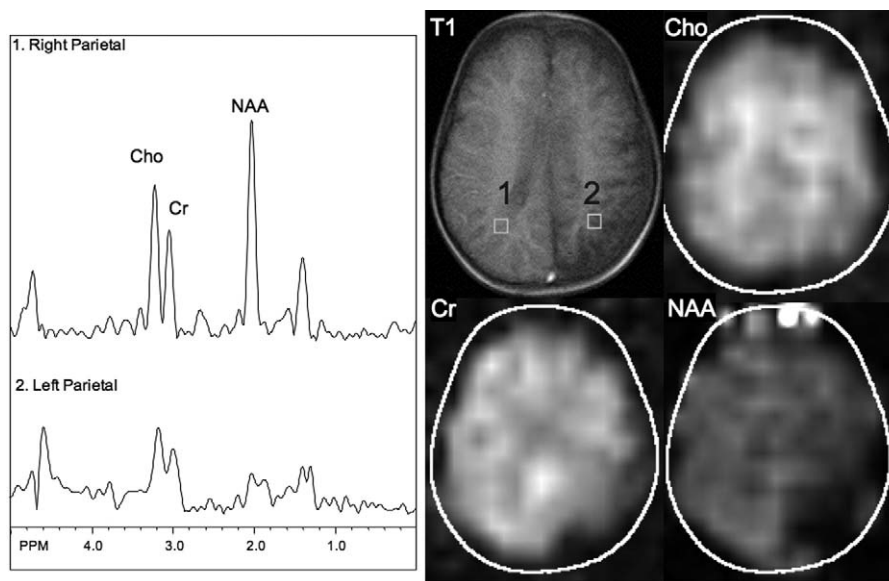**Figure 26** Magnetic resonance spectroscopic imaging (MRSI) of the same girl as in Figure 25. Corresponding to atrophic left parietal lobe, there is reduction of all metabolites (Cho, choline), in part reflecting volume averaging with adjacent CSF. In addition, the NAA is markedly diminished reflecting neuronal loss or dysfunction.
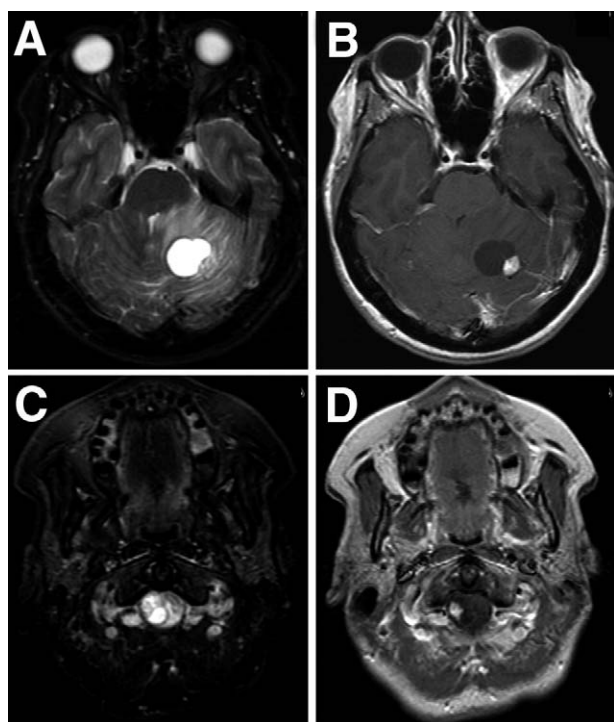

Figure 27 A 23-year-old woman with VHL presenting with head-ache. (A) Axial T2-weighted and (B) post-GdDTPA T1-weighted images show a left cerebellar cystic mass with an enhancing mural nodule, associated with surrounding vasogenic edema, compression of the left dorsolateral pons, and effacement of the fourth ventricle. (C) Axial T2-weighted and (D) post-GdDTPA T1-weighted images at the level of the C1-2 junction show another mixed cystic and solid mass in the right aspect of the cord. Both tumors were hemangioblastomas.
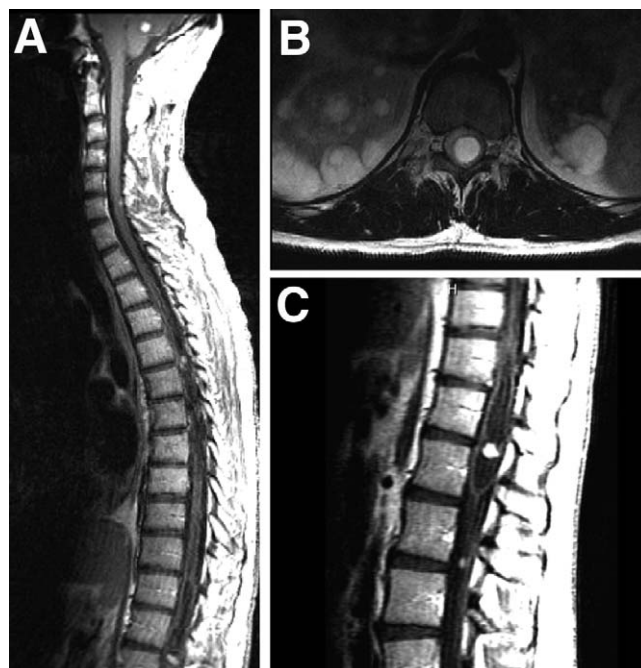
Figure 28 A 30-year-old man with VHL. (A) A post-GdDTPA sagittal T1 weighted image shows multiple enhancing hemangioblastomas in the cerebellum and within the cord. (B) An axial T2-weighted image shows a peripherally located intramedullary cystic hemangioblastoma expanding the cord. Multiple cystic masses are present in the kidneys. (C) Magnified view of the conus shows a cystic hemangioblastoma with a central enhancing solid nodule and another small solidly enhancing one in the proximal filum.

Figure 29 A 38-year-old woman with VHL, presenting with left-sided tinnitus and hearing loss. (A) An axial CT image of the left temporal bone and (B) coronal CT image of both sides show a soft-tissue mass centered in the left cerebellopontine angle causing lytic destruction of the petrous temporal bone. The soft-tissue mass also extends to the tympanic cavity. The mass was resected with histology revealing endolymphatic sac tumor.
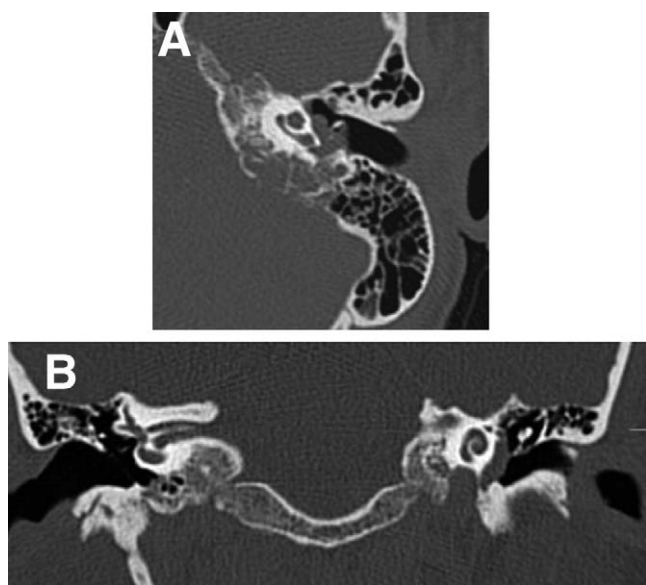
hemangioblastomas (44%-72%), spinal hemangioblastomas (13%-50%), and retinal angiomas (25%-60%).[77] Outside the CNS, there is also multisystem involvement including renal cysts that have a high incidence of developing into clear-cell renal cell carcinomas, pancreatic cysts and neuroendocrine tumors, pheochromocytomas, and epididymal or broad ligament papillary cystadenomas.

In the CNS, hemangioblastoma occurs most frequently in the cerebellum.[77,82] It arises from endothelial origin and is very vascular. Initially, hemangioblastoma shows solid enhancement and appears pial based and is therefore peripherally located in the cerebellum. When large, its appearance is most often cystic with an enhancing mural nodule (Fig 27), and the natural history of progression shows a faster rate of cystic expansion than growth of the causative solid tumor, eventually resulting in pressure effect and clinical symptoms.[83,84] At times, hemorrhage or prominent serpiginous vascular flow voids can be found associated with the tumor. Although solitary cerebellar hamangioblastoma can occur in any individual, multiplicity suggests the syndrome of VHL. Small tumors are often seen as solidly enhancing nodules that may be difficult to distinguish from metastatic disease.

Hemangioblastoma also occurs in the brainstem with a similar appearance, and in the spine as intramedullary lesions. Because of the peripheral, pial-based location, at times, it is difficult to classify tumor location as intramedullary or extramedullary. Focal expansile T2 hyperintense mass with solid enhancement (25%) or cystic with an enhancing nodule is the typical appearance (Fig 28). There may also be associated syrinx within the cord.[84]

Although rare, endolymphatic sac tumors occur with higher frequency in VHL individuals, affecting about 10% of patients.[85,86] This is a very vascular and locally aggressive tumor that arises from the endolymphatic sac, which often causes lytic erosion of the petrous temporal bone resulting in sensorineural hearing loss, disequilibrium, and aural fullness (Fig 29).[85,87,88]

Summary

In summary, neuroimaging plays an important role in the diagnosis of the phakomatoses. Conventional, morphologic imaging techniques such as CT scans and MRI document CNS involvement including lesion size, distribution, and location; newer "functional" imaging techniques (for instance based on perfusion or metabolism) offer further insights into disease pathophysiology.

References

1. Korf BR: The phakomatoses. Neuroimaging Clin N Am 14:139-148, 2004
2. Friedman JM: Epidemiology of neurofibromatosis type 1. Am J Med Genet 89:1-6, 1999
3. Cichowski K, Jacks T: NF1 tumor suppressor gene function: narrowing the GAP. Cell 104:593-604, 2001
4. World Health Organization Classification of Tumors, Pathology & Geneics. Lyon: IARC Press, 2000
5. Friedrich RE, Korf B, Funsterer C, et al: Growth type of plexiform neurofibromas in NF1 determined on magnetic resonance images. Anticancer Res 23:949-952, 2003
6. Rodriguez D, Young Poussaint T: Neuroimaging findings in neurofibromatosis type 1 and 2. Neuroimaging Clin N Am 14:149-170, 2004
7. Evans DG, Baser ME, McGaughran J, et al: Malignant peripheral nerve sheath tumours in neurofibromatosis 1. J Med Genet 39:311-314, 2002
8. Solomon SB, Semih Dogan A, Nicol TL, et al: Positron emission tomography in the detection and management of sarcomatous transformation in neurofibromatosis. Clin Nucl Med 26:525-528, 2001
9. Cardona S, Schwarzbach M, Hinz U, et al: Evaluation of F18-deoxyglucose positron emission tomography (FDG-PET) to assess the nature of neurogenic tumours. Eur J Surg Oncol 29:536-541, 2003
10. Ferner RE, Lucas JD, O'Doherty MJ, et al: Evaluation of (18)fluorodeoxyglucose positron emission tomography ((18)FDG PET) in the detection of malignant peripheral nerve sheath tumours arising from within plexiform neurofibromas in neurofibromatosis 1. J Neurol Neurosurg Psychiatry 68:353-357, 2000
11. Friedman JM, Birch PH: Type 1 neurofibromatosis: a descriptive analysis of the disorder in 1,728 patients. Am J Med Genet 70:138-143, 1997
12. Balcer LJ, Liu GT, Heller G, et al: Visual loss in children with neurofibromatosis type 1 and optic pathway gliomas: relation to tumor location by magnetic resonance imaging. Am J Ophthalmol 131:442-445, 2001
13. Griffiths PD, Blaser S, Mukonoweshuro W, et al: Neurofibromatosis bright objects in children with neurofibromatosis type 1: a proliferative potential? Pediatrics 104:e49, 1999
14. Itoh T, Magnaldi S, White RM, et al: Neurofibromatosis type 1: the evolution of deep gray and white matter MR abnormalities. AJNR Am J Neuroradiol 15:1513-1519, 1994
15. Van Es S, North KN, McHugh K, et al: MRI findings in children with neurofibromatosis type 1: a prospective study. Pediatr Radiol 26:478-487, 1996
16. DiPaolo DP, Zimmerman RA, Rorke LB, et al: Neurofibromatosis type 1: pathologic substrate of high-signal-intensity foci in the brain. Radiology 195:721-724, 1995
17. Kraut MA, Gerring JP, Cooper KL, et al: Longitudinal evolution of

unidentified bright objects in children with neurofibromatosis-1. Am J Med Genet A 129:113-119, 2004

18. Denckla MB, Hofman K, Mazzocco MM, et al: Relationship between T2-weighted hyperintensities (unidentified bright objects) and lower IQs in children with neurofibromatosis-1. Am J Med Genet 67:98-102, 1996

19. North KN, Riccardi V, Samango-Sprouse C, et al: Cognitive function and academic performance in neurofibromatosis. 1: consensus statement from the NF1 Cognitive Disorders Task Force. Neurology 48: 1121-1127, 1997

20. Cutting LE, Koth CW, Burnette CP, et al: Relationship of cognitive functioning, whole brain volumes, and T2-weighted hyperintensities in neurofibromatosis-1. J Child Neurol 15:157-160, 2000

21. Evans DG: Neurofibromatosis type 2: genetic and clinical features. Ear Nose Throat J 78:97-100, 1999

22. Evans DG, Lye R, Neary W, et al: Probability of bilateral disease in people presenting with a unilateral vestibular schwannoma. J Neurol Neurosurg Psychiatry 66:764-767, 1999

23. National Institutes of Health Consensus Development Conference Statement on Acoustic Neuroma, December 11-13, 1991. The Consensus Development Panel. Arch Neurol 51:201-207, 1994

24. Baser ME, Friedman JM, Wallace AJ, et al: Evaluation of clinical diagnostic criteria for neurofibromatosis 2. Neurology 59:1759-1765, 2002

25. Rouleau GA, Merel P, Lutchman M, et al: Alteration in a new gene encoding a putative membrane-organizing protein causes neuro-fibromatosis type 2. Nature 363:515-521, 1993

26. Trofatter JA, MacCollin MM, Rutter JL, et al: A novel moesin-, ezrin-, radixin-like gene is a candidate for the neurofibromatosis 2 tumor suppressor. Cell 72:791-800, 1993

27. Smirniotopoulos JG, Murphy FM: The phakomatoses. AJNR Am J Neuroradiol 13:725-746, 1992

28. Patronas NJ, Courcoutsakis N, Bromley CM, et al: Intramedullary and spinal canal tumors in patients with neurofibromatosis 2: MR imaging findings and correlation with genotype. Radiology 218:434-442, 2001

29. Mautner VF, Friedrich RE, von Deimling A, et al: Malignant peripheral nerve sheath tumours in neurofibromatosis type 1: MRI supports the diagnosis of malignant plexiform neurofibroma. Neuroradiology 45: 618-625, 2003

30. Thiele EA: Managing epilepsy in tuberous sclerosis complex. J Child Neurol 19:680-686, 2004

31. Prather P, de Vries PJ: Behavioral and cognitive aspects of tuberous sclerosis complex. J Child Neurol 19:666-674, 2004

32. Goh S, Kwiatkowski DJ, Dorer DJ, et al: Infantile spasms and intellectual outcomes in children with tuberous sclerosis complex. Neurology 65:235-238, 2005

33. Roach ES, Sparagana SP: Diagnosis of tuberous sclerosis complex. J Child Neurol 19:643-649, 2004

34. van Slegtenhorst M, de Hoogt R, Hermans C, et al: Identification of the tuberous sclerosis gene TSC1 on chromosome 9q34. Science 277:805-808, 1997

35. Identification and characterization of the tuberous sclerosis gene on chromosome 16. The European Chromosome 16 Tuberous Sclerosis Consortium. Cell 75:1305-1315, 1993

36. Narayanan V: Tuberous sclerosis complex: genetics to pathogenesis. Pediatr Neurol 29:404-409, 2003

37. van Slegtenhorst M, Nellist M, Nagelkerken B, et al: Interaction between hamartin and tuberin, the TSC1 and TSC2 gene products. Hum Mol Genet 7:1053-1057, 1998

38. Christophe C, Sekhara T, Rypens F, et al: MRI spectrum of cortical malformations in tuberous sclerosis complex. Brain Dev 22:487-493, 2000

39. DiMario FJ Jr: Brain abnormalities in tuberous sclerosis complex. J Child Neurol 19:650-657, 2004

40. Griffiths PD, Martland TR: Tuberous sclerosis complex: the role of neuroradiology. Neuropediatrics 28:244-252, 1997

41. Shepherd CW, Houser OW, Gomez MR: MR findings in tuberous sclerosis complex and correlation with seizure development and mental impairment. AJNR Am J Neuroradiol 16:149-155, 1995

42. Roach ES, Gomez MR, Northrup H: Tuberous sclerosis complex con-sensus conference: revised clinical diagnostic criteria. J Child Neurol 13:624-628, 1998

43. Iwasaki S, Nakagawa H, Kichikawa K, et al: MR and CT of tuberous sclerosis: linear abnormalities in the cerebral white matter. AJNR Am J Neuroradiol 11:1029-1034, 1990

44. Griffiths PD, Bolton P, Verity C: White matter abnormalities in tuberous sclerosis complex. Acta Radiol 39:482-486, 1998

45. Christophe C, Bartholome J, Blum D, et al: Neonatal tuberous sclerosis. US, CT, and MR diagnosis of brain and cardiac lesions. Pediatr Radiol 19:446-448, 1989

46. Smirniotopoulos JG: Neuroimaging of phakomatoses: Sturge-Weber syndrome, tuberous sclerosis, von Hippel-Lindau syndrome. Neuroimaging Clin N Am 14:171-183, 2004

47. Griffiths PD, Gardner SA, Smith M, et al: Hemimegalencephaly and focal megalencephaly in tuberous sclerosis complex. AJNR Am J Neuroradiol 19:1935-1938, 1998

48. Tarasow E, Kubas B, Walecki J: MR proton spectroscopy in patients with CNS involvement in Bourneville's disease. Med Sci Monit 7:762-765, 2001

49. Mukonoweshuro W, Wilkinson ID, Griffiths PD: Proton MR spectroscopy of cortical tubers in adults with tuberous sclerosis complex. AJNR Am J Neuroradiol 22:1920-1925, 2001

50. Yapici Z, Dincer A, Eraksoy M: Proton spectroscopic findings in children with epilepsy owing to tuberous sclerosis complex. J Child Neurol 20:517-522, 2005

51. Garaci FG, Floris R, Bozzao A, et al: Increased brain apparent diffusion coefficient in tuberous sclerosis. Radiology 232:461-465, 2004

52. Karadag D, Mentzel HJ, Gullmar D, et al: Diffusion tensor imaging in children and adolescents with tuberous sclerosis. Pediatr Radiol 35: 980-983, 2005

53. Jansen FE, Braun KP, van Nieuwenhuizen O, et al: Diffusion-weighted magnetic resonance imaging and identification of the epileptogenic tuber in patients with tuberous sclerosis. Arch Neurol 60:1580-1584, 2003

54. Sieg KG, Harty JR, Simmons M, et al: Tc-99m HMPAO SPECT imaging of the central nervous system in tuberous sclerosis. Clin Nucl Med 16:665-667, 1991

55. Rintahaka PJ, Chugani HT: Clinical role of positron emission tomography in children with tuberous sclerosis complex. J Child Neurol 12:42-52, 1997

56. Moore GJ, Slovis TL, Chugani HT: Proton magnetic resonance spectroscopy in children with Sturge-Weber syndrome. J Child Neurol 13:332-335, 1998

57. Kagawa K, Chugani DC, Asano E, et al: Epilepsy surgery outcome in children with tuberous sclerosis complex evaluated with alpha-[11C]methyl-L-tryptophan positron emission tomography (PET). J Child Neurol 20:429-438, 2005

58. Maria BL, Hoang KB, Robertson RL, et al: Imaging Brain Structure and Function in Sturge-Weber Syndrome. Mt Freedom, NJ, Sturge-Weber Foundation, 1999

59. Comi AM: Pathophysiology of Sturge-Weber syndrome. J Child Neurol 18:509-516, 2003

60. Thomas-Sohl KA, Vaslow DF, Maria BL: Sturge-Weber syndrome: a review. Pediatr Neurol 30:303-310, 2004

61. Enjolras O, Riche MC, Merland JJ: Facial port-wine stains and Sturge-Weber syndrome. Pediatrics 76:48-51, 1985

62. Roach ES: Neurocutaneous syndromes. Pediatr Clin North Am 39:591-620, 1992

63. Griffiths PD: Sturge-Weber syndrome revisited: the role of neuroradiology. Neuropediatrics 27:284-294, 1996

64. Marti-Bonmati L, Menor F, Poyatos C, et al: Diagnosis of Sturge-Weber syndrome: comparison of the efficacy of CT and MR imaging in 14 cases. AJR Am J Roentgenol 158:867-871, 1992

65. Wasenko JJ, Rosenbloom SA, Duchesneau PM, et al: The Sturge-Weber syndrome: comparison of MR and CT characteristics. AJNR Am J Neuroradiol 11:131-134, 1990

66. Bebin EM, Gomez MR: Prognosis in Sturge-Weber disease: comparison of unihemispheric and bihemispheric involvement. J Child Neurol 3:181-184, 1988

67. Griffiths PD, Coley SC, Romanowski CA, et al: Contrast-enhanced fluid-attenuated inversion recovery imaging for leptomeningeal disease in children. AJNR Am J Neuroradiol 24:719-723, 2003

68. Reichenbach JR, Barth M, Haacke EM, et al: High-resolution MR venography at 3.0 Tesla. J Comput Assist Tomogr 24:949-957, 2000

69. Reichenbach JR, Jonetz-Mentzel L, Fitzek C, et al: High-resolution blood oxygen-level dependent MR venography (HRBV): a new technique. Neuroradiology 43:364-369, 2001

70. Mentzel HJ, Dieckmann A, Fitzek C, et al: Early diagnosis of cerebral involvement in Sturge-Weber syndrome using high-resolution BOLD MR venography. Pediatr Radiol 35:85-90, 2005

71. Griffiths PD, Boodram MB, Blaser S, et al: 99mTechnetium HMPAO imaging in children with the Sturge-Weber syndrome: a study of nine cases with CT and MRI correlation. Neuroradiology 39:219-224, 1997

72. Bar-Sever Z, Connolly LP, Barnes PD, et al: Technetium-99m-HMPAO SPECT in Sturge-Weber syndrome. J Nucl Med 37:81-83, 1996

73. Reid DE, Maria BL, Drane WE, et al: Central nervous system perfusion and metabolism abnormalities in Sturge-Weber syndrome. J Child Neurol 12:218-222, 1997

74. Maria BL, Neufeld JA, Rosainz LC, et al: Central nervous system structure and function in Sturge-Weber syndrome: evidence of neurologic and radiologic progression. J Child Neurol 13:606-618, 1998

75. Lin DD, Barker PB, Kraut MA, et al: Early characteristics of Sturge-Weber syndrome shown by perfusion MR imaging and proton MR spectroscopic imaging. AJNR Am J Neuroradiol 24:1912-1915, 2003

76. Breiter SN, Arroyo S, Mathews VP, et al: Proton MR spectroscopy in patients with seizure disorders. AJNR Am J Neuroradiol 15:373-384, 1994

77. Lonser RR, Glenn GM, Walther M, et al: von Hippel-Lindau disease. Lancet 361:2059-2067, 2003

78. Sims KB: Von Hippel-Lindau disease: gene to bedside. Curr Opin Neurol 14:695-703, 2001

79. Maher ER, Iselius L, Yates JR, et al: Von Hippel-Lindau disease: a genetic study. J Med Genet 28:443-447, 1991

80. Latif F, Tory K, Gnarra J, et al: Identification of the von Hippel-Lindau disease tumor suppressor gene. Science 260:1317-1320, 1993

81. Barry RE, Krek W: The von Hippel-Lindau tumour suppressor: a multifaceted inhibitor of tumourigenesis. Trends Mol Med 10:466-472, 2004

82. Choyke PL, Glenn GM, Walther MM, et al: von Hippel-Lindau disease: genetic, clinical, and imaging features. Radiology 194:629-642, 1995

83. Slater A, Moore NR, Huson SM: The natural history of cerebellar hemangioblastomas in von Hippel-Lindau disease. AJNR Am J Neuroradiol 24:1570-1574, 2003

84. Wanebo JE, Lonser RR, Glenn GM, et al: The natural history of hemangioblastomas of the central nervous system in patients with von Hippel-Lindau disease. J Neurosurg 98:82-94, 2003

85. Choo D, Shotland L, Mastroianni M, et al: Endolymphatic sac tumors in von Hippel-Lindau disease. J Neurosurg 100:480-487, 2004

86. Lonser RR, Kim HJ, Butman JA, et al: Tumors of the endolymphatic sac in von Hippel-Lindau disease. N Engl J Med 350:2481-2486, 2004

87. Devaney KO, Ferlito A, Rinaldo A: Endolymphatic sac tumor (low-grade papillary adenocarcinoma) of the temporal bone. Acta Otolaryngol 123:1022-1026, 2003

88. Kim HJ, Butman JA, Brewer C, et al: Tumors of the endolymphatic sac in patients with von Hippel-Lindau disease: implications for their natural history, diagnosis, and treatment. J Neurosurg 102:503-512, 2005